Human Molecular Genetics, 2021, Vol. 30, No. 17 1591–1606

https://doi.org/10.1093/hmg/ddab142
Advance Access Publication Date: 27 May 2021
General Article

GENERAL ARTICLE

Comprehensive phenotypic and functional analysis of dominant and recessive *FOXE3* alleles in ocular developmental disorders

Linda M. Reis[1,†], Elena A. Sorokina[1,†], Lubica Dudakova[2], Jana Moravikova[2], Pavlina Skalicka[2,3], Frantisek Malinka[2,4], Sarah E. Seese[1], Samuel Thompson[1], Tanya Bardakjian[5], Jenina Capasso[6], William Allen[7], Tom Glaser[8], Alex V. Levin[6], Adele Schneider[5], Ayesha Khan[9,10], Petra Liskova[2,3] and Elena V. Semina[1,11,*]

[1]Department of Pediatrics, Children's Research Institute at the Medical College of Wisconsin and Children's Hospital of Wisconsin, Milwaukee, WI 53226, USA, [2]Department of Pediatrics and Inherited Metabolic Disorders, First Faculty of Medicine, Charles University and General University Hospital, 121 08 Prague, Czech Republic, [3]Department of Ophthalmology, First Faculty of Medicine, Charles University and General University Hospital, 121 08 Prague, Czech Republic, [4]Department of Computer Science, Czech Technical University in Prague, 166 36 Prague, Czech Republic, [5]Department of Pediatrics, Albert Einstein Medical Center, Philadelphia, PA 19141, USA, [6]Pediatric Ophthalmology and Ocular Genetics, Flaum Eye Institute, Pediatric Genetics, Golisano Children's Hospital, University of Rochester, Rochester, NY 14534 USA, [7]Fullerton Genetics Center, Mission Hospitals, HCA, Asheville, NC 28803 USA, [8]Cell Biology and Human Anatomy Department, UC-Davis School of Medicine, Davis, CA 95616, USA, [9]Pediatric Ophthalmology and Strabismus Unit, Al-Shifa Trust Eye Hospital, Rawalpindi, Pakistan, [10]Pediatric Ophthalmologist, Al Jalila Children's Specialty Hospital, Dubai, United Arab Emirates and [11]Departments of Ophthalmology and Visual Sciences and Cell Biology, Neurobiology and Anatomy, Medical College of Wisconsin, Milwaukee, WI 53226, USA

*To whom correspondence should be addressed. Tel: +414 9552218; Fax: +414 9550025; Email: esemina@mcw.edu

Abstract

The forkhead transcription factor *FOXE3* is critical for vertebrate eye development. Recessive and dominant variants cause human ocular disease but the full range of phenotypes and mechanisms of action for the two classes of variants are unknown. We identified *FOXE3* variants in individuals with congenital eye malformations and carried out *in vitro* functional analysis on selected alleles. Sixteen new recessive and dominant families, including six novel variants, were identified. Analysis of new and previously reported genetic and clinical data demonstrated a broad phenotypic range with an overlap between recessive and dominant disease. Most families with recessive alleles, composed of truncating and forkhead-domain missense variants, had severe corneal opacity (90%; sclerocornea in 47%), aphakia (83%) and microphthalmia (80%), but

[†]Equal contribution

Received: March 23, 2021. **Revised:** May 18, 2021. **Accepted:** May 19, 2021

some had milder features including isolated cataract. The phenotype was most variable for recessive missense variants, suggesting that the functional consequences may be highly dependent on the type of amino acid substitution and its position. When assessed, aniridia or iris hypoplasia were noted in 89% and optic nerve anomalies in 60% of recessive cases, indicating that these defects are also common and may be underrecognized. In dominant pedigrees, caused by extension variants, normal eye size (96%), cataracts (99%) and variable anterior segment anomalies were seen in most, but some individuals had microphthalmia, aphakia or sclerocornea, more typical of recessive disease. Functional studies identified variable effects on the protein stability, DNA binding, nuclear localization and transcriptional activity for recessive *FOXE3* variants, whereas dominant alleles showed severe impairment in all areas and dominant-negative characteristics.

Introduction

The *FOXE3* transcription factor, a member of the forkhead box (Fox) family, is important for vertebrate lens development (1–3). Fox proteins share a highly conserved winged-helix DNA-binding domain (forkhead domain, FHD) and are divided into subgroups (A-S) based on sequence similarity both within and outside the domain. Phylogenetically, FoxE proteins most closely resemble the FoxD family (4). The Fox protein subclasses have distinct non-forkhead domains, binding partners, cofactors, spatiotemporal expression patterns and developmental roles. The FoxE family consists of *Foxe1*, associated with thyroid and palatal development, and *Foxe3* (4). Despite the fact that ocular expression of *Foxe3* in mouse embryos is limited to the lens (2,3), both mice and humans carrying *FOXE3* variants display complex ocular phenotypes including anterior segment anomalies and/or microphthalmia in addition to lens anomalies (1–3,5,6).

Pathogenic *FOXE3* variants can cause dominant or recessive eye phenotypes. The first reported pathogenic variant, in an individual with posterior embryotoxon, cataracts and myopia (OMIM #610256), was a heterozygous frameshift mutation near the stop codon, which removed the five C-terminal residues and added an erroneous tail extending past the native stop codon by 111 amino acids (1). Subsequently, three independent heterozygous extension variants were found in families with anterior segment dysgenesis (ASD) and/or congenital cataracts (7–9); these variants occur within the stop codon and append a different 72–amino acid tail. Heterozygous missense variants in the forkhead domain were also reported in a family with Peters anomaly and a simplex case with syndromic cataracts, respectively (5,10); an additional heterozygous missense variant [c.146G > C p.(Gly49Ala)] was initially reported to be causative in a family with ocular disease but later shown to be a population-specific variant (7,11).

A second class of *FOXE3* variants with recessive phenotypes was subsequently identified in individuals with aphakia, microphthalmia and/or sclerocornea (OMIM #610256) (6) and were homozygous in many cases (associated with consanguinity). These alleles include missense variants within the forkhead domain and frameshift or nonsense variants that truncate the protein (6,7,11–13). Heterozygous carriers are typically unaffected, suggesting that the two types of variants have different cellular or developmental properties. Current functional data are limited and do not distinguish these classes (14). Importantly, the *FOXE3* gene contains a single exon; its mRNA is unspliced, so truncating variants would not be expected to trigger nonsense-mediated decay resulting in normal expression of the mutant mRNA and corresponding protein.

In this study, we report 16 new families with pathogenic recessive (14) or dominant (2) *FOXE3* alleles, including 6 novel variants. To determine their mechanism of action, we functionally characterized two dominant and four recessive alleles *in vitro*.

Results

FOXE3 recessive alleles and phenotypes

By screening subjects with anterior eye malformations, we identified recessive *FOXE3* pathogenic or likely pathogenic variants in 22 individuals from 14 families (Table 1; Figs 1 and 2; Supplementary Material, Supplementary Data; Supplementary Material, Fig. S1). All variants were absent or rare (<0.02%) with no homozygotes detected in gnomAD (Table 1). Sclerocornea or another corneal opacity was the most consistent feature, reported in all but one (Individual 5) subject with available data. Most affected individuals had microphthalmia though bilateral normal eye size was noted in four patients and microphthalmia was unilateral in five; of note, all individuals with normal eye size also had a diagnosis of glaucoma, raising the possibility that increased intraocular pressure modified the eye size. The corneal opacity was typically dense, significantly limiting vision and precluding any view of the anterior segment. Primary aphakia was observed in all individuals in whom lens phenotypes could be assessed except in one case with congenital cataract (Individual 5). Less commonly identified features involved iris anomalies, reported in every case where this feature was examined, optic nerve atrophy (one) and optic nerve coloboma (one). Clinical features were typically limited to ocular anomalies, but in one family (Individuals 9A and 9B), intellectual disability and autism were also present; genetic investigation (clinical microarray and research exome analysis of OMIM genes) did not identify an alternative explanation for the cognitive phenotype.

Twelve different variants were identified, six of which were novel. Seven alleles were missense variants affecting the forkhead domain; four alleles were frameshift and one was nonsense. The novel missense variants had CADD scores >25 and REVEL scores >0.5, indicating likely pathogenicity. The novel frameshift variants c.148_170dup p.(Gly58Argfs*174), c.543del p.(Pro182Argfs*42) and c.844_850dup p.(Glu284Alafs*3) met ACMG criteria to be considered pathogenic (PVS1, PM2, PM3, PP4, ±PP1; see Supplementary Material, Supplementary Data for specific details), while the novel missense alleles c.286G > A p.(Ala96Thr), c.359G > C p.(Arg120Pro) and c.371C > T p.(Thr124Met) were considered likely pathogenic (PM1, PM2, PM3, PP2, PP3, PP4, ±PP1 and PM5; see Supplementary Material, Supplementary Data for specific details). The previously reported missense allele c.244A > G p.(Met82Val) (15) was most common, detected in three families. Other recurrent alleles included the c.21_24del p.(Met7Ilefs*216), c.232G > A p.(Ala78Thr) and c.720C > A p.(Cys240*) variants and the novel c.371C > T p.(Thr124Met) allele.

Table 1. Phenotypic and genetic information for new *FOXE3* cases reported in this paper

Indiv ID[a]	Age; origin	Zygosity	Nucleotide change[b]	Predicted effect	MAF[c]	*In silico* analysis[d]	CADD/REVEL[e]	Globe size	Cornea	Lens	Iris	Other	Ref
Recessive pathogenic alleles													
1	1y; SA	Hom	c.21_24del	p.(Met7Ilefs*216)	1/65918	Truncation	–	Severe MI	Severe corneal opacity, microcornea	U	U	ON coloboma	(7)
2A	U; SA	Hom[f]	c.21_24del	p.(Met7Ilefs*216)	1/65918	Truncation	–	MI	Sclerocornea	U	U	NYS	(7)
2B	U; SA	Hom[f]	c.21_24del	p.(Met7Ilefs*216)	1/65918	Truncation	–	MI	Sclerocornea	U	U	NYS	(7)
2C	U; SA	Hom[f]	c.21_24del	p.(Met7Ilefs*216)	1/65918	Truncation	–	MI	Sclerocornea	U	U	NYS	(7)
3	**3m; SA**	**Hom**	**c.148_170dup**	**p.(Gly58Argfs*174)**	**NP (~26 000)**	**Truncation**	–	**Left MI**	**Corneal opacity, microcornea**	**Primary aphakia**	**IH, ICA**	**CGL**	–
4	**5m; W/A**	**C Het**	c.232G > A	p.(Ala78Thr)	10/248542	Dam. 5/5	24.8/0.862	**MI (L > R)**	**Complete corneal opacity L microcornea**	**R primary aphakia; L lens remnant attached to cornea**	**No view**	**CGL**	(15)
			c.286G > A	**p.(Ala96Thr)**	**NP (276924)**	**Dam. 4/5**	**26.2/0.515**						–
5	31y; U	C Het	c.232G > A	p.(Ala78Thr)	10/248542	Dam. 5/5	24.8/0.862	R mild MI	L microcornea	L anterior polar CAT	L IH	ASD, CGL	(7)
			c.244A > G	p.(Met82Val)	24/264152	Dam. 5/5	23.8/0.875						(7)
6	16y; SA	Hom	c.244A > G	p.(Met82Val);	24/264152	Dam. 5/5	23.8 0.875	MI	Sclerocornea	Primary aphakia	Aniridia		(7)
7A	**25y; W**	**C Het**	c.244A > G	p.(Met82Val)	24/264152	Dam. 5/5	23.8/0.875	**L MI**	**Sclerocornea**	**No view**	**No view**	**GL, NYS**	(15)
			c.543del	**p.(Pro182Argfs*42)**	**NP (~50 000)**	**Truncation**	–						–
7B	**31y; W**	**C Het**	c.244A > G	p.(Met82Val)	24/264152	Dam. 5/5	23.8/0.875	**MI**	**Sclerocornea**	**Primary aphakia**	**No view**	**NYS**	(15)
			c.543del	**p.(Pro182Argfs*42)**	**NP (~50 000)**	**Truncation**	–						–
8	U; SA	Hom	c.289A > G	p.(Ile97Val)	5/247928	Dam. 5/5	24.9/0.775	MI	U	U	U	U	(25)
9A	13y; L	Hom	c.291C > G	p.(Ile97Met)	5/248080	Dam. 5/5	24.2/0.750	L MI	Corneal opacity	No view	No view	ON atrophy, R CGL	(22)
9B	9y; L	Hom	c.291C > G	p.(Ile97Met)	5/248080	Dam. 5/5	24.2/0.750	R severe MI	Corneal opacity	No view	No view	CGL, R phthisis	(22)
10A	**6y; ME**	**Hom**	**c.359G > C**	**p.(Arg120Pro)**	**NP (250050)**	**Dam. 5/5**	**32.0/0.933**	–	Sclerocornea	Primary aphakia	U	CGL	–
10B	**10m; ME**	**Hom**	**c.359G > C**	**p.(Arg120Pro)**	**NP (250050)**	**Dam. 5/5**	**32.0/0.933**	–	**Sclerocornea**	**No view**	**U**	**CGL**	–
10C	**2y; ME**	**Hom**	**c.359G > C**	**p.(Arg120Pro)**	**NP (250050)**	**Dam. 5/5**	**32.0/0.933**	–	**Sclerocornea**	**Primary aphakia**	**U**	**CGL**	–
11A	**37y; EA**	**C Het**	**c.371C > T**	**p.(Thr124Met)**	**9/278804**	**Dam. 5/5**	**25.3/0.772**	**MI**	**Sclerocornea**	**R primary aphakia**	**U**	**U**	–
			c.844_850dup	**p.(Glu284Alafs*3)**	**3/30540**	**Truncation**	–						–
11B	**38y; EA**	**C Het**	**c.371C > T**	**p.(Thr124Met)**	**9/278804**	**Dam. 5/5**	**25.3/0.772**	**MI**	**Sclerocornea**	**U**	**U**	**U**	–
			c.844_850dup	**p.(Glu284Alafs*3)**	**3/30540**	**Truncation**	–						–
12	**8m; EA**	**Hom**	**c.371C > T**	**p.(Thr124Met)**	**9/278804**	**Dam. 5/5**	**25.3/0.772**	**– (at birth)**	**Sclerocornea**	**Primary aphakia**	**Aniridia**	**CGL**	–
13	13y; EA	Hom	c.720C > A	p.(Cys240*)	7/43132	Truncation	36/–	MI	Sclerocornea	Primary aphakia	U	U	(6)
14A	3y; SA	Hom	c.720C > A	p.(Cys240*)	7/43132	Truncation	36/–	MI	U	U	U	U	(6)
14B	U; SA	Hom	c.720C > A	p.(Cys240*)	7/43132	Truncation	36/–	MI	U	U	U	U	(6)
Dominant pathogenic alleles													
15A	59y; W	Het	c.959G > C	p.(*320Serext*72)	NP (~31 000)	Extension	15.12/–	–	PE	CAT (SX 29-30y)	Corectopia, mild IH, ICA	GL	(8)
15B	39y; W	Het	c.959G > C	p.(*320Serext*72)	NP (~31 000)	Extension	15.12/–	–	U	CCAT (SX 28y)	U	GL	(8)
15C	57y; W	Het	c.959G > C	p.(*320Serext*72)	NP (~31 000)	Extension	15.12/–	–	Sclerocornea	U	U	U	(8)
15D	87y; W	Het	c.959G > C	p.(*320Serext*72)	NP (~31 000)	Extension	15.12/–	–	Mild microcornea	CCAT (SX 38y)	Mild IH	GL	(8)
16A	40y; W	Het	c.958 T > C	p.(*320Argext*72)	NP (~31 000)	Extension	17.52/–	–	PE	CCAT (SX 24y)	mild IH	–	(7)
16B	3.5y; W	Het	c.958 T > C	p.(*320Argext*72)	NP (~31 000)	Extension	17.52/–	–	Sclerocornea	No view	No view	NYS	(7)
16C	55y; W	Het	c.958 T > C	p.(*320Argext*72)	NP (~31 000)	Extension	17.52/–	–	PE	CAT (SX 33y)	mild IH	U	(7)
16D	20y; W	Het	c.958 T > C	p.(*320Argext*72)	NP (~31 000)	Extension	17.52/–	–	PE	CAT (SX 29y)	ICA, mild IH	U	(7)
16E	76y; W	Het	c.958 T > C	p.(*320Argext*72)	NP (~31 000)	Extension	17.52/–	–	U	CAT (SX 30s)	U	U	(7)

[a]Unrelated families have consecutive numbers; members of the same family are labeled with A–E.
[b]Based on NM_012186.3.
[c]Frequency in gnomAD (no homozygotes present for any variant).
[d]SIFT, Polyphen2, Mutation Assessor, Mutation Taster, FATHMM-MKL (from dbNSFP v4.1a accessed through VEP): Dam.-predicted damaging/deleterious.
[e]CADDphred and REVEL scores (from dbNSFP v4.1a accessed through VEP); CADD score > 20 and REVEL score > 0.5 indicates predicted pathogenicity.
[f]Presumed homozygous (consanguineous).
Bold alleles are novel. Eye anomalies are bilateral unless specified. ASD, anterior segment dysgenesis; C, congenital; CAT, cataract; GL, glaucoma; ICA, iridocorneal adhesions; IH, iris hypoplasia; L, left; MI, microphthalmia; NS, not specified; NYS, nystagmus; ON, optic nerve; PE, posterior embryotoxon; R, right; SX, surgery; U,unknown; A, Asian; EA, East Asian; L, Latino; ME, Middle Eastern; SA, South Asian; W, White. Ref. is previous report of the identified mutation in another family.

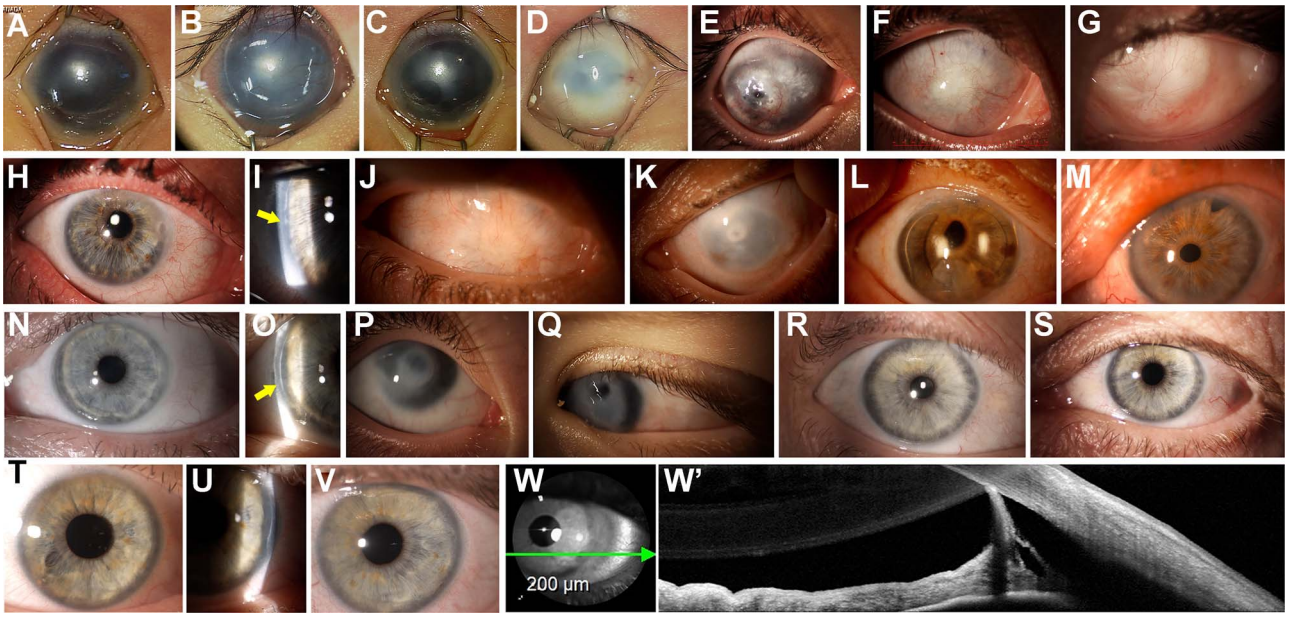

Figure 1. Ocular features associated with *FOXE3* variants. (**A–W**) Ocular photographs. Individual 12 (right, A, B; left, C, D) at 1 month (A, C) and 6 months (B, D) showing aniridia and silvery gray appearance to cornea typical of *FOXE3* (A–C) along with acquired phthisis of right eye (D); Individuals 7A (right, E) and 7B (right, F, left G) showing corneal opacity (7B underwent bilateral keratoplasty); Individual 15A (right, H, I) showing corectopia and mild iris hypoplasia as well as posterior embryotoxon (I, yellow arrow); Individual 15C (right, J, left, K) showing sclerocornea; Individual 15D (right, L, left, M) showing mild iris hypoplasia and posterior embryotoxon; Individual 16A (left, N, O) with mild iris hypoplasia and posterior embryotoxon temporally (yellow arrow); Individual 16B (right, P; left, Q) showing sclerocornea with central clearing; Individuals 16C (right, R; left, S) and 16D (right T, U; left, V) showing posterior embryotoxon temporally and nasally and mild iris hypoplasia. (W) Ocular image of Individual 16D taken just prior to OCT imaging of the iridocorneal angle. (**W'**) OCT imaging of Individual 16D showing temporal iridocorneal adhesion.

In ten families, the variant was homozygous (with known consanguinity in seven); compound heterozygous variants were identified in the remaining four. Biallelic truncating variants were identified in five families, while biallelic missense variants were identified in seven, and *trans* missense and truncating variants were found in the remaining two families (Supplementary Material, Fig. S1). Affected individuals with biallelic missense variants were more likely to have at least one normal sized eye (7/10), associated with early glaucoma, compared to those with biallelic truncating variants (1/8). While iris hypoplasia or aniridia was reported in four individuals with missense variants, significant corneal opacity precluded assessment of the anterior segments in most individuals.

Including these new cases, clinical and genetic information has been reported for 111 individuals from 49 families with biallelic *FOXE3* variants (Supplementary Material, Table S1, Fig. 3) (6,7,11–27). In order to avoid skewing from variability in family size, we counted each family once using an average frequency of various features within the family and then averaged the frequency of features by the number of families assessed for each feature; since corneal opacity often precluded examination of the anterior segment, lens and retina, for these features, the number of families assessed is lower.

Corneal opacity was the most consistent feature, seen in 90% of those with data available; sclerocornea was specifically noted in 46.6%, Peters anomaly in 7.5%, other severe corneal opacity in 26.1%, mild to moderate corneal opacity in 10.6%, and no details regarding the opacity were available for 9.2%. Aphakia was seen in 83% and cataract was noted in 17% (though lens phenotype was only assessed in 29 families). Finally, bilateral microphthalmia was noted in 64.2%, asymmetric microphthalmia (with normal eye size of contralateral eye) in 15.6% and bilateral normal eye size in 20.2%. Interestingly, glaucoma was noted in 32/34 normal sized eyes with data available; glaucoma was also reported in some microphthalmic eyes. While iris anomalies were only reported in 16 individuals from 14 families, this is primarily due to a lack of view of the anterior segment in most cases. Among families where the iris was specifically assessed, iris anomalies were noted in 89%, including aniridia/absent iris in 31.3%. Similarly, optic nerve anomalies such as coloboma or hypoplasia were only reported in 9 families but were seen in 60% of those in whom the posterior segment was assessed, and other retinal anomalies, notably retinal detachment, were occasionally reported. The vast majority of *FOXE3* cases have isolated ocular findings, but syndromic anomalies are noted in some cases. The only recurrent anomaly was intellectual disability/developmental delay, noted in Individuals 9A and 9B and in four previous case reports (7,11,15,16). In four of the five families, the *FOXE3* variant was homozygous and truncating variants were present in three.

In order to determine whether missense alleles have a milder effect compared to truncating variants, we compared clinical features in all reported families. Overall, biallelic missense variants were identified in 64 individuals from 25 families, while biallelic truncating variants were seen in 39 individuals from 18 families; the remaining 6 families had a combination of missense and truncating variants (5) or an in-frame deletion (1). Using normalized family data, we compared those with biallelic missense variants to those with biallelic truncating variants (Fig. 3). While cataract and lack of corneal opacity were only seen in families with biallelic missense variants, this difference approached but did not reach statistical significance ($P = 0.14$ and $P = 0.07$, respectively). Increased frequency of at least one normal sized eye (typically associated with glaucoma) within the biallelic missense group also approached significance ($P = 0.0504$). While assessed in fewer individuals, the rates of glaucoma, iris

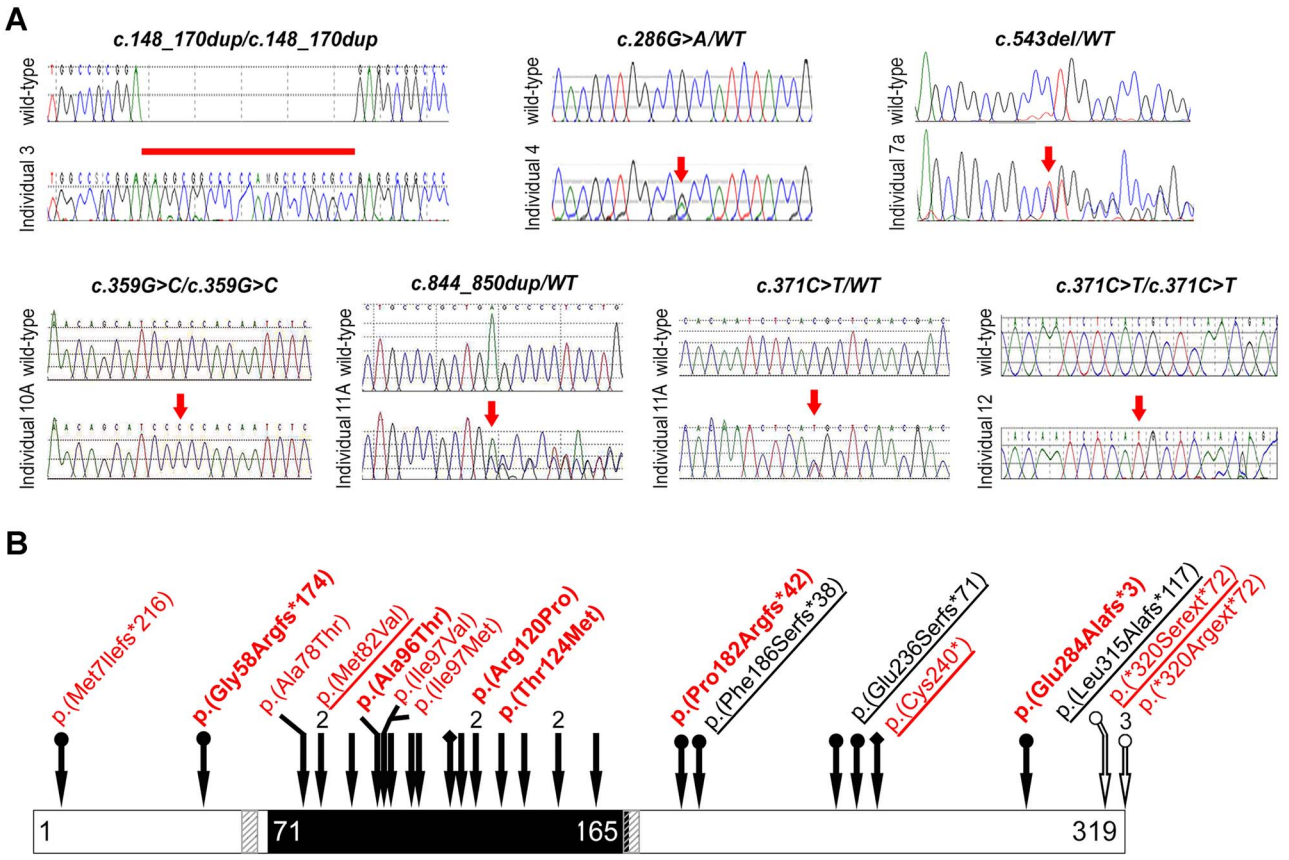

Figure 2. FOXE3 variant summary. (**A**) Sanger chromatogram traces for novel *FOXE3* variants identified in this study. In each panel, the normal sequence is shown on the top and variant location is marked in red. (**B**) Schematic of *FOXE3* protein with pathogenic alleles indicated. Red text, alleles reported in this study; bold (red) text, novel alleles in this study; underlined text, alleles with functional analysis presented in this study. Filled black arrows, recessive alleles; empty arrows, dominant alleles. Arrow top circles, frameshift; diamonds, truncation; no symbol, missense allele. Numbers above arrows indicate the number of unique variants at that position. Black box indicates the forkhead domain (amino acids 71–165); striped gray boxes correspond to the two predicted nuclear localization signals at amino acid positions 57–66 and 162–170.

anomalies and optic nerve phenotypes were similar in both groups (80.3% versus 79.2%; 81.3% versus 96.4; 40% versus 57.5%, respectively). Overall, the phenotype associated with missense variants was the most variable, ranging from a severe disease indistinguishable from truncating variants to milder presentations; the majority of individuals with clear corneas and isolated cataract had one of two missense variants, c.307G > A p.(Glu103Lys) or c.351C > G p.(Asn117Lys) (17,20), suggesting that the functional consequences may be highly dependent on the type of amino acid substitution and its position.

Among recessive families, most alleles are unique or rare, affecting only one or two families, but several were seen more frequently. Including the new cases reported here, the c.21_24del p.(Met7llefs*216) and c.720C > A p.(Cys240*) alleles are reported in six and nine families, respectively, with homozygous cases and South Asian ancestry suggesting remote founder effects. Likewise, the c.232G > A p.(Ala78Thr) allele was seen in four families, three with compound heterozygosity; two families with reported ethnicity were European but the allele is seen in both European and Latino populations in gnomAD samples. The similar c.244A > G p.(Met82Val) allele, reported in eight families, is seen in diverse populations in both affected families and gnomAD samples. The novel c.371C > T p.(Thr124Met) allele appears to be more common in East Asian populations and several other alleles reported in two or three families also had carriers identified among ethnically matched populations in gnomAD (Supplementary Material, Table S1). Fourteen recessive alleles are not present in gnomAD, while the remaining 13 have a low carrier frequency (less than 1 in 10 000) with no homozygotes.

FOXE3-dominant alleles and phenotypes

Two dominant pathogenic extension alleles were identified in nine individuals from two families (Fig. 1), both previously reported and neither present in gnomAD (Table 1; Fig. 2). These are two different extension alleles, which modify the stop codon (TGA > TCA, TGA > CGA) but preserve the frame, adding a 72–amino acid nonsense peptide to the C-terminus. While CADD scores are lower for these variants (15–17), the CADD score only assesses the effect at the site of the change and does not consider the effect of the erroneous protein tail that extends the length of the protein. The dominant pathogenic variants resulted in cataracts in all cases where the lens could be evaluated. The cataracts typically did not require removal until early/middle adulthood. Affected family members were aphakic at the time of evaluation so no details regarding the specific cataract phenotype were available. Eye size was normal in all individuals, but mild anterior segment anomalies affecting the cornea and/or iris were noted in some individuals. Sclerocornea was observed in two family members (15C and 16B). This finding is typical for individuals with recessive *FOXE3* variants, but no

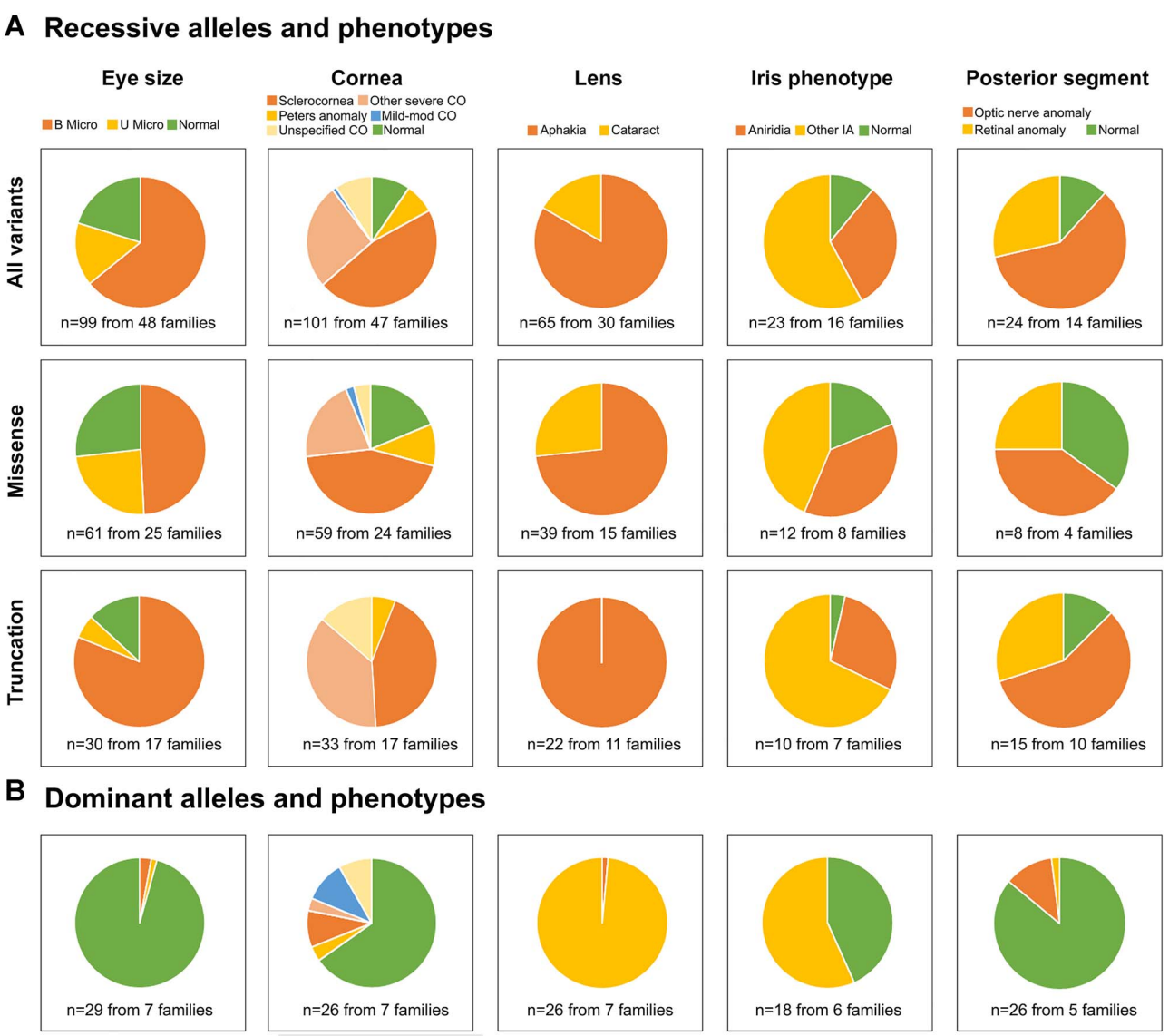

Figure 3. Summary of phenotypic features in all patients with *FOXE3* variants. (**A**) Pie charts showing distribution of features among families with all recessive alleles, only biallelic missense, or only biallelic truncating variants. (**B**) Pie charts showing distribution of features among families with dominant extension alleles. Ocular features were normalized by family by averaging the features within each family and then averaging across all families; percentages were calculated based on the number of individuals assessed for each feature. B bilateral; U unilateral; CO corneal opacity; IA iris anomaly.

second pathogenic variant in the single exon *FOXE3* gene was identified *in trans* in either case.

Including these new cases, heterozygous extension alleles were identified in 29 individuals from 7 families (Supplementary Material, Table S2) (1,7–9,28). Three distinct variants change the stop codon into a codon for Leu, Ser or Arg in six independent families, extending the reading frame by 72 codons, and one frameshift allele alters the six C-terminal codons and incorporates an erroneous tail extending past the native stop codon by 111 amino acids (in the +1 reading frame). Using normalized family data, as described above, we determined the distribution of features. In almost all cases, cataract (98.6%) and normal eye size (95.7%) were seen but bilateral microphthalmia with unilateral aphakia was reported in one individual. Surgical removal of cataracts was typically not required until adulthood (20–40 years). Corneal opacities were occasionally reported including Peters anomaly (3.75%), sclerocornea (9.2%), other severe corneal opacity (3.1%) and unspecified corneal opacity (8.3%), and milder corneal scleralization was noted in an additional 10.4%; other corneal anomalies were also reported but inconsistently assessed including posterior embryotoxon and microcornea. Iris anomalies were common, reported in 56.7%, and consisted of mild iris hypoplasia, iris coloboma and/or iridocorneal adhesions. Posterior segment anomalies were rare, but optic disk coloboma and retinal detachment were occasionally seen.

Ocular phenotypes have also been occasionally reported in individuals with heterozygous missense alleles in the *FOXE3* forkhead domain, which would be expected to result in recessive disease (Supplementary Material, Table S2) (5,10,29), and one heterozygous parent in a recessive family (c.557del variant) had unilateral corneal cloudiness and decreased visual acuity

(11); however, in two other cases with a *FOXE3* heterozygous missense or a small in-frame duplication variant, an alternative genetic cause was identified (8,15). These recessive heterozygous alleles may predispose individuals to cataracts and corneal disease but require environmental or genetic 'second hits' for expression or these individuals may simply be carriers of recessive alleles with an unrelated explanation for their ocular phenotype.

Molecular modeling wild-type and mutant FOXE3 proteins

At the present time, the experimentally determined structure of FOXE3 is not available, but several other FHD structures with similarity to FOXE3 exceeding 60% were resolved including rat Foxd3 (30), human FOXC2 (31) and human FOXA2 (32). The FHD sequence is highly conserved for all members of the Fox family. It generally consists of three main alpha-helices, two or three beta-strands and one or two loops termed 'wings'. Helix 3 (H3) is the location of the major groove DNA-contact and it is responsible for the specificity of binding (30) and helix 1 (H1) is involved in maintaining the conformation of the FHD necessary for transactivation (33). A small additional 3_{10} helix 4 sometimes forms downstream of helix 2 with a hinge loop separating these structures. The H2 and H4 juxtaposed helices are known to merge into one upon domain swapping and dimerization in the forkhead box P family (34).

We performed *ab initio* molecular modeling of wild-type FOXE3 as well as recessive (p.Met82Val, p.Phe186Serfs*38, p.Glu236Serfs*71, p.Cys240*) and dominant (p.Leu315Alafs*117 and p.*320Serext*72) variants (Supplementary Material, Fig. S2); functional analysis was also performed for these six alleles, which will hereafter be referred to using their short format, where applicable (i.e. p.Phe186fs, p.Glu236fs, p.Leu315fs and p.*320ext). The full-length wild-type protein contains an FHD (amino acids (aa) 71–165), with important DNA-binding activity, and two predicted nuclear localization signals (NLS), at aa57–66 and aa162–170 flanking the FHD. Structurally, the FHD is predicted to contain two antiparallel β-sheet strands (termed β-hairpin; aa129–147) and four α-helices (α1 aa76–86; α2 aa94–102; α3 aa112–125; α4 aa149–157). C-terminal to the FHD, three small additional alpha helices are found (aa175–178, aa227–232, aa254–256).

In the structure predicted for the p.Met82Val protein, the β-hairpin and α4 structures are notably lost within the FHD, α2 is elongated and a small α-helix between α2 and α3 is added. Outside of the FHD, the three native α-helices are reduced in length, and five small new α-helices (aa32–35, aa43–47, aa222–225, aa242–246, aa287–289) are predicted, slightly altering the overall tertiary fold. For p.Glu236fs, the protein truncation is predicted to disrupt α3, remove α4 and add an α-helix between α2 and α3 within the FHD. Due to the frameshift and premature truncation, only one α-helix remains outside the FHD (aa174–178). For p.Phe186fs, the protein truncates shortly after the second NLS; within the FHD, this results in a loss of α4, an elongation of α2 and an additional α-helix between α2 and α3. Due to the frameshift and premature truncation, all secondary structures outside of the FHD are lost. For p.Cys240*, the FHD is largely similar to wild-type, with a slight elongation of α2 and an additional small α-helix observed between α2 and α3. However, all native α-helices outside the FHD were lost; only one small α-helix, aa215–217, was predicted. Finally, for both dominant variants p.*320ext and p.Leu315fs, almost all secondary and tertiary structures are lost throughout the protein, resulting in a highly unrecognizable structure in comparison to the wild-type.

Expression and subcellular localization of mutant FOXE3 proteins

Wild-type and mutant FOXE3 proteins (Fig. 4A), detected by western blot analysis using an N-terminal FLAG tag, were variably expressed following transient transfection with equal amounts of expression plasmids (Fig. 4B and C). Recessive mutant p.Met82Val was expressed similarly to wild-type, but p.Cys240*, p.Phe186fs and p.Glu236fs proteins were markedly decreased (64%, 4% and 32%, respectively). Dominant variants p.Leu315fs and p.*320ext also showed reduced protein levels (26% and 32% of wild-type, respectively) (Fig. 4B and C). In a parallel RT-PCR experiment, the level of *FOXE3* mRNA was similar in all samples (Fig. 4B). These results suggest that the analyzed frameshift and extension mutants are relatively instable.

To assess subcellular localization of mutant proteins, we immunostained transfected cells for the N-terminal FLAG epitope. The FOXE3 proteins were primarily nuclear, but cytoplasmic staining was significantly increased for all mutants except p.Glu236fs (Fig. 4D and E), despite retention of both NLS motifs. The percentage of FLAG+ cells with cytoplasmic staining was highest for the dominant mutants, particularly p.Leu315fs (25%).

DNA-binding activity of FOXE3 variants

To test the DNA-binding activity of wild-type and mutant FOXE3 proteins, we performed EMSA using a dsDNA oligonucleotide probe [referred to as FHB (forkhead binding) that contains a consensus binding site of the closely related forkhead protein FOXD3 (4) (GATTG**TTT**GTTT)] (35) or a mismatch derivative, FHBmut (GATTG**CCC**GTTT) (Fig. 5A). In these experiments, wild-type FOXE3 interacted strongly with FHB, forming three DNA-protein complexes (one major and two minor) of slower mobility; no binding was observed with the mismatch probe (Fig. 5A). Minimal binding was observed with untransfected HLE-B3 cell extracts, presumably reflecting low-level expression of endogenous FOX protein(s). A supershift assay with N-terminal antibody confirmed the specificity of FOXE3 binding in all three DNA-protein complexes (Fig. 5A).

To investigate how *FOXE3* pathogenic variants affect DNA binding, we performed EMSA with proteins corresponding to recessive (p.Met82Val, p.Phe186fs, p.Glu236fs, p.Cys240*) and dominant (p.Leu315fs and p.*320ext) variants. Since several variants were associated with decreased expression (Fig. 4B and C), we adjusted the amount of plasmid DNA in each transfection to achieve similar FOXE3 protein levels (Fig. 5B and C). Among recessive mutants, p.Met82Val had noticeably reduced DNA-binding capacity, whereas p.Glu236fs and p.Phe186fs bound FHB similarly to wild-type, and p.Cys240* demonstrated a slightly increased binding capability (Fig. 5B). Both dominant mutants (p.Leu315fs and p.*320ext) showed moderately reduced binding (Fig. 5C). These results are consistent with *ab initio* molecular modeling of recessive mutants, which predicted p.Met82Val and p.Cys240* to have the greatest and least change in FHD structure, respectively. However, the moderate binding of both dominant extension mutants to FHB probe was surprising given the highly disorganized structures predicted by I-Tasser (Supplementary Material, Fig. S2). These observations illustrate the limitations of *ab initio* predictions and the intrinsic robustness of FHD folding *in vivo*.

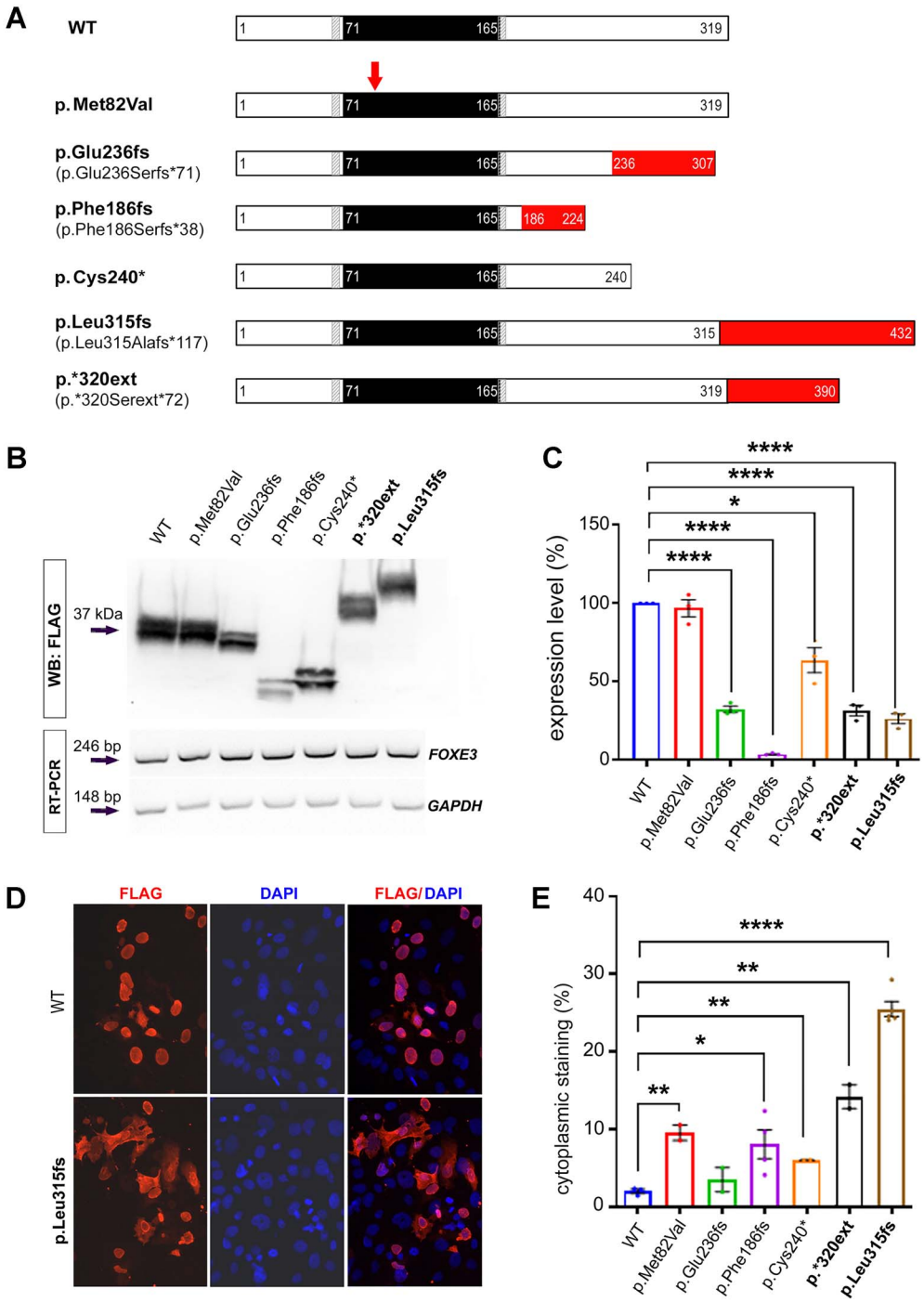

Figure 4. FOXE3 proteins and their western blot analysis and subcellular localization. (**A**) Diagram of wild-type (WT) and mutant FOXE3 proteins used in functional studies. Full and short names (in parenthesis, when applicable) are given for all variants. Black box, forkhead domain; striped gray boxes, two predicted nuclear localization signals at amino acid positions 57–66 and aa162–170; red arrow, location of missense variant; red box, erroneous tail introduced by frameshift or extension mutation. (**B**) Nuclear extracts from HLE-B3 cells transiently transfected with plasmids encoding WT or mutant FOXE3 proteins with N-terminal FLAG tag, and RT-PCRs for FOXE3 and GADPH, performed with RNA from a parallel transfection. FOXE3 proteins migrate as doublets, reflecting possible posttranslation modification. (**C**) Quantification of western blot signals. Most mutant FOXE3 proteins are less abundant than WT despite similar transcript levels. (**D**) Subcellular localization of ^{FLAG}FOXE3 proteins, revealed by anti-FLAG and DAPI staining. WT FOXE3 is nuclear, whereas the p.Leu315Alafs*117 mutant is cytoplasmic in ~25% of cells. (**E**) Quantitation of FLAG+ cells with cytoplasmic staining. Most FOXE3 mutants exhibit significant cytoplasmic localization. Dominant alleles are indicated with bold font. Error bars show standard error of the mean (SEM). Statistical significance is indicated by asterisks as *, $P < 0.05$; **, $P < 0.01$; ****, $P < 0.0001$.

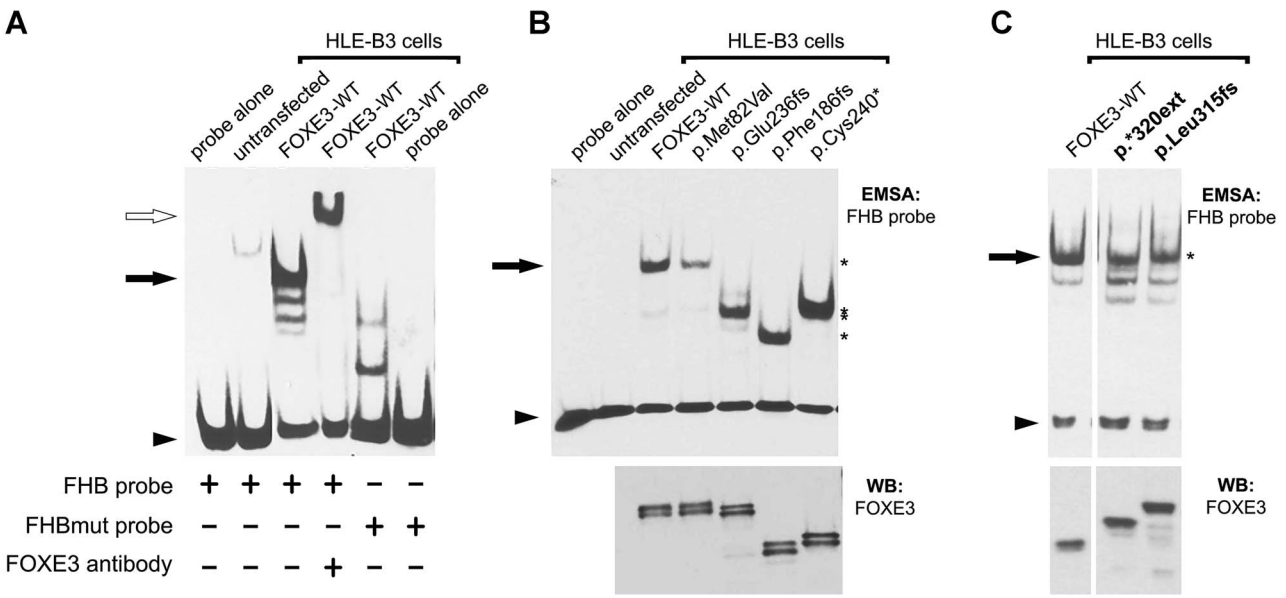

Figure 5. Electrophoretic mobility shift assays (EMSA) of FOXE3 proteins in transfected HLE-B3 cell extracts. (**A**) Wild-type FOXE3 binds the FHB probe, forming four complexes of differing mobility. The slowest moving complex (black arrow, lane 3) accounts for most of the shifted probe; unbound probe is indicated with an arrowhead. N-terminal FOXE3 antibody supershifts all complexes (open arrow, lane 4), validating the specificity of the FOXE3-FHB binding. Mutated probe FHBmut does not produce the same complexes (lane 5). (**B**) Binding of recessive FOXE3 variant proteins to the FHB probe was markedly reduced for one mutant, p.Met82Val (asterisks on the right indicate positions of the corresponding protein-DNA complexes). (**C**) Dominant variant FOXE3 proteins bind the FHB probe with moderately reduced affinity (major complexes indicated with asterisk). Western blots (WB) in lower panels show comparable abundance of FOXE3 protein in cell extracts.

FOXE3 protein dimerization studies

Some forkhead-domain proteins self-associate to form homodimers (34,36–39). To investigate the dimerization of wild-type and mutant FOXE3 proteins, and the potential for dominant-negative molecular effects, we coexpressed ^{FLAG}FOXE3 variants with wild-type FOXE3^{myc} and performed parallel coimmunoprecipitation (co-IP) assays on cell extracts with mouse anti-FLAG, anti-myc or control IgG (Fig. 6). The precipitated proteins were detected in western blots using goat anti-FOXE3 sera and were distinguished by the reduced mobility of FLAG- versus myc-tagged isoforms. In these reciprocal experiments, wild-type FOXE3^{myc} was coimmunoprecipitated with every ^{FLAG}FOXE3 mutant, but the anti-Myc co-IPs were somewhat less efficient. Although the interacting proteins were overexpressed *in transfecto*, our results suggest that FOXE3 proteins may self-interact (dimerize) *in vivo*.

Transactivation by variant FOXE3 proteins

The transcriptional activity of wild-type and variant FOXE3 proteins was tested in parallel luciferase cotransfection assays using the $(FHB)_6$-TK-luc reporter in lens epithelial (HLE-B3) and embryonic kidney (HEK293) cell lines. Transfections were performed with mutant and wild-type constructs, alone and in combination, adjusting the amount of expression plasmid to achieve comparable protein levels for each variant (Fig. 7A and B).

All variants differed significantly in their transactivation ability compared to wild-type FOXE3. Wild-type FOXE3 activated luciferase expression 1.8-fold in HLE-B3 cells and 3.6-fold in HEK293 cells compared to pcDNA3.1 vector controls. p.Met82Val and p.Glu236fs*71 were less potent, activating luciferase 1.3-fold in HLE-B3 (both mutants) and 1.2- or 0.9-fold in HEK293, respectively. At the same time, p.Cys240* was more potent, activating luciferase 5.2-fold in HLE-B3 and 4.9-fold in HEK293, whereas p.Phe186fs*38 had mixed effects [4.0-fold in HLE-B3 but 1.2-fold in HEK293 (Fig. 7A)].

The transcriptional effects were most pronounced for the two dominant mutants, which expressed less luciferase than the controls, 0.7- to 0.9-fold in HLE-B3 and 0.3-fold in HEK293 (Fig. 7A). To evaluate dominant-negative effects, we performed similar assays with mutant and wild-type FOXE3 proteins coexpressed in approximately equal ratios. In these mixing experiments, combinations involving recessive mutants gave intermediate luciferase levels, but combinations involving dominant mutants consistently resulted in low luciferase levels, at or below negative controls, even with added wild-type FOXE3, 0.85- to 1.0-fold in HLE-B3 and 0.5- to 0.6-fold in HEK 293, for p.Leu315fs and p.*320ext variants, respectively (Fig. 7B). These results suggest that the extension alleles have dominant-negative effects on transcription.

Discussion

These data confirm the role of recessive *FOXE3* pathogenic variants in microphthalmia associated with primary aphakia and sclerocornea, and dominant pathogenic extension variants in cataracts with variable milder anterior segment dysgenesis. Extraocular features were noted in only one family among 16 in our study, and all carriers of recessive alleles were unaffected.

Including the new families reported here, there are now 27 different recessive *FOXE3* pathogenic variants identified in 49 unrelated families. While truncating alleles were less common (9/27 unique alleles), they were more likely to occur in multiple families, so 41/98 disease alleles were truncating, while 57/98 were missense (56) or in-frame deletion (1) alleles. Primary aphakia with corneal opacity and microphthalmia is the typical recessive phenotype, but occasional patients with biallelic variants are reported with dominant-like features of cataract

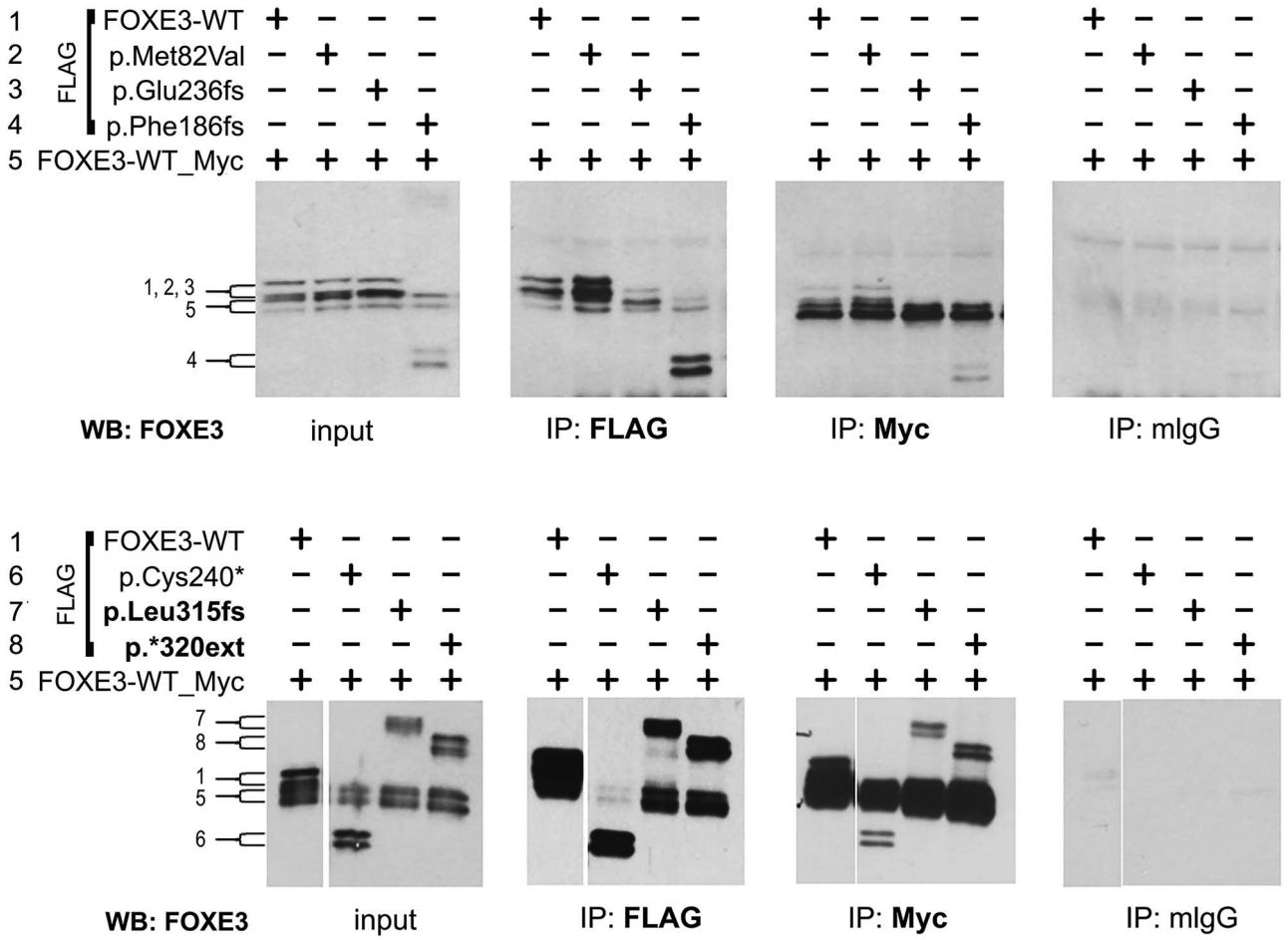

Figure 6. Dimerization of FOXE3 proteins. FLAG-tagged mutant or WT FOXE3 proteins were coexpressed with myc-tagged WT FOXE3, immunoprecipitated in parallel with anti-MYC, anti-FLAG or normal mouse IgG and analyzed by western blotting with anti-FOXE3 antibody. The precipitation of both proteins in each lane suggests that WT FOXE3 can dimerize with itself and every FOXE3 mutant tested. Numbers 1–8 indicate the positions of different FOXE3 proteins, identified above the gels.

without corneal opacity, typically with one of two specific missense alleles [c.307G > A p.(Glu103Lys) and c.351C > G p.(Asn117Lys)]. Underrecognized associations include normal eye size (unilateral or bilateral) in the context of early-onset glaucoma, iris anomalies and optic nerve anomalies. Given dense corneal opacities, full clinical assessment of *FOXE3* defects requires alternative imaging modalities, such as ultrasound, optical coherence tomography (OCT), or magnetic resonance imaging (MRI) to diagnose; thus, the complete spectrum of *FOXE3* ocular defects in many affected individuals may not be fully identified. In prior studies, all individuals with primary aphakia undergoing penetrating keratoplasty were found to have atrophic iris tissue, suggesting that the absence of the lens disrupts iris development; however, since no genetic analysis was performed, the causative variant(s) in these cases may directly affect development of both structures (40). Indeed, mouse models (*dysgenic lens*, *Foxe3*^{dyl}) support a role for *Foxe3* in iris development; *Foxe3*+/− mice have intact lens epithelia but hypoplastic iris tissue and iridocorneal and iridolenticular adhesions (41).

Most cases with *FOXE3* variants have isolated ocular findings; the only recurrent syndromic anomaly was intellectual disability or developmental delay, now noted in five families with recessive disease. While the frequency of intellectual disability in families with recessive *FOXE3* variants is elevated (5/49 families, 11%), this may represent the increased risk of intellectual disability among offspring of consanguineous parents (42) given that homozygous variants were noted in four of these five families. However, direct neurological effects cannot be ruled out since mouse *Foxe3* is expressed in the presumptive midbrain of mouse embryos (2,3). A role for *FOXE3* outside the eye was further supported by a reported association of heterozygous missense variants in the C-terminal region of the FHD with transthoracic aortic aneurysms and dissections (TAAD) (43); to date, TAAD has not been reported in patients with ocular disease, but only one ocular variant [c.47G > C p.(Gly158Arg)] falls within the TAAD region. It is not clear whether these variants have distinct effects on FOXE3 function or if ocular patients may develop TAAD at a later age (average age of presentation for TAAD was 46 years). Additional data are needed regarding this association.

Including families reported here, dominant extension variants have been reported in 29 individuals from 7 families. Three distinct variants affect the stop codon in six independent families and the fourth variant occurs slightly upstream but results in a similar length erroneous tail. Typical ocular anomalies consisted of cataract, usually visually insignificant until adulthood, and mild anterior segment anomalies. Interestingly, in almost all families, some family members have a more severe corneal phenotype, resembling recessive disease, suggesting that unknown modifiers play an important role in determining phenotype.

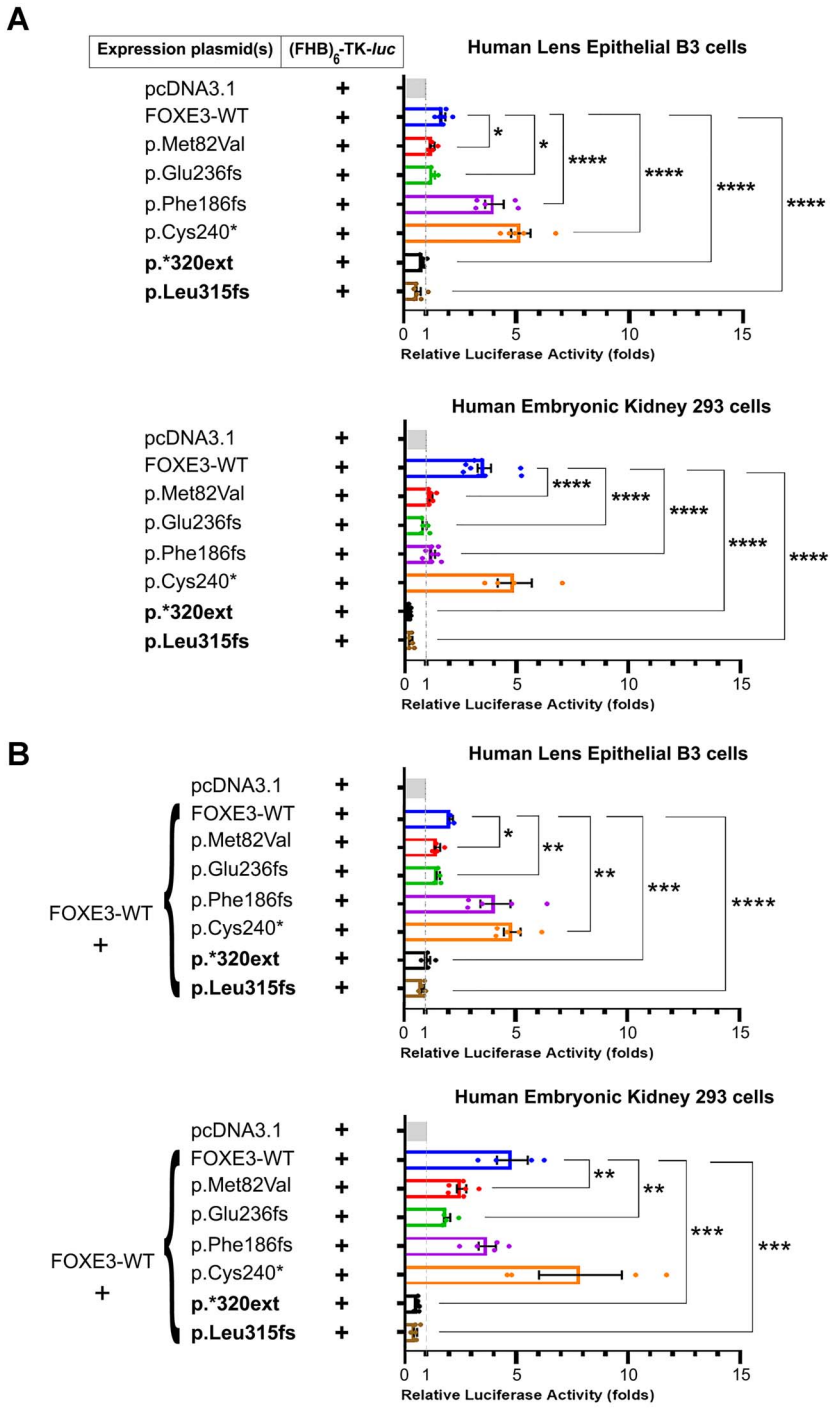

Figure 7. Luciferase assays of FOXE3 transcriptional activity. (**A**) HLE-B3 and HEK293 cells were transfected with $(FHB)_6$-TK-luc plasmid and the FOXE3 expression vectors indicated. Bar graphs show fold activation over empty pcDNA3.1 vector. Each mutant is significantly different than WT, with dominant alleles having no activity. (**B**) Adding WT FOXE3 increased the transcriptional activity of all reactions, but mutant levels still differ from WT, and the activity of dominant alleles is lower than control (empty pcDNA3.1 vector, gray line at 1.0). Error bars show SEM. Statistical significance is indicated by asterisks as *, $P < 0.05$; **, $P < 0.01$; ***, $P < 0.001$; ****, $P < 0.0001$.

A role for modifiers is further supported by the presence of rare heterozygous missense variants of uncertain significance in patients with ocular disease. A similar phenomenon is observed in mice: complete deficiency of *Foxe3* in mice results in the *dysgenetic lens (dyl)* phenotype, characterized by microphthalmia and major anterior segment anomalies (2,3), but a proportion of heterozygotes have corneal and lens defects resembling Peters anomaly (5). Additionally, one previous study found a common SNP, c.601G > A p.Val201Met, was enriched among cases with eye malformations (18).

In vitro data show dominant extension alleles severely disrupt FOXE3 functions, decreasing protein stability and DNA

binding, increasing cytoplasmic localization and abolishing transcriptional activity. In contrast, the recessive alleles had variable effects. Every allele tested but one (p.Met82Val) had reduced stability (most pronounced for p.Phe186fs) and all but one (p.Glu236fs) had moderate cytoplasmic localization. However, only one mutant (p.Met82Val) had markedly reduced DNA binding and two (p.Met82Val and p.Glu236fs) had uniformly decreased transcriptional activity. Indeed, two mutants (p.Cys240*, p.Phe186fs) had greater activity than wild-type in one or both cell lines tested.

Our findings contrast with prior functional studies of four recessive (p.Arg90Leu; p.Met7llefs*216; p.Arg120Gly; p.Glu 236Serfs*71) and two dominant (p.*320Argext∗72; p.Leu315Al afs*117) *FOXE3* alleles (14), which noted strict nuclear localization for all mutants and robust DNA binding to a FOXC1 consensus site (GATCCAAAGTAAATAAACAACAGA) by dominant and one recessive mutant (p.Arg90Leu) but no binding by the three other recessive mutants (44). Using a HeLa luciferase reporter assay that included a *FOXO1* promoter segment, these authors showed that recessive mutants had 39–66% of the wild-type FOXE3 activity, whereas dominant mutants retained 75% of wild-type activity, without dominant-negative effects. Only two alleles overlap between these studies and the experiments used different binding sequences and cell lines. We used a consensus sequence for FOXD3, which is phylogenetically closer to FOXE3 (4) and performed assays in human lens cells, which are physiologically relevant. Of note, our luciferase results for one mutant differed between the two cell lines tested here.

Some FOX transcription factors self-interact, forming homo- or heterodimers. Dimerization was demonstrated for FOXP proteins but has been considered a unique feature of this family, since it requires an alanine residue in a specific position within the FHD hinge loop, which allows subunits to swap domains (34,45). In other FHDs, the corresponding residue is proline, except for FOXE3 (ala) FOXS1 (ala) and FOXJ1 (cys), raising the possibility that these proteins undergo similar dimerization. Our data suggest that wild-type FOXE3 can dimerize with wild-type and mutant FOXE3 proteins. If FOXE3 dimers form *in vivo*, this may exacerbate the deleterious effects of pathogenic variants in heterozygous carriers, particularly for extension variants, which appear to act as dominant-negative alleles.

Overall, this study significantly increases (by 40%) the number of families reported with pathogenic *FOXE3* variants, both dominant and recessive. In general, truncating and FHD missense variants in *FOXE3* are recessive but extension alleles, which add an erroneous protein tail beyond the native stop codon, are dominant. However, phenotypes vary significantly, with overlap between recessive and dominant ocular features. Functional data show variable disruption of protein stability, subcellular localization, DNA binding and transactivation for recessive alleles and severe impairment for dominant extension alleles.

Materials and Methods

Human subjects

This study was approved by the Institutional Review Boards of the Children's Hospital of Wisconsin, Medical College of Wisconsin and General University Hospital in Prague, including sample collection protocols at Einstein Healthcare Network, Wills Eye Hospital and the University of Iowa. Written informed consent was provided by all participants and/or their legal guardians, including permission to publish photographs, as applicable. DNA was extracted from blood or saliva samples following standard procedures. Cases with *FOXE3* variants were identified through genetic screening (below) of study populations with developmental ocular anomalies. Literature review of reported *FOXE3* variants (Supplementary Material, Tables S1 and S2) was completed using HGMD (46) and PubMed (pubmed.ncbi.nlm.nih.gov). In order to avoid skewing due to discrepant family size, ocular features were normalized by family by averaging the features within each family and then averaging across all families. Not all features are noted for every individual, so all percentages were calculated based on the number of individuals assessed for each feature. Family members without genetic testing results reported or with insufficient clinical description were excluded from the analysis. For cases with corneal opacity, if a specific diagnosis was not provided, cases were categorized as 'other severe corneal opacity' if noted as 'complete' or 'opaque', if visual acuity was reported as perception of light or worse, or if reported to have no view of the anterior segment. Statistical analysis of features seen in families with biallelic missense versus biallelic truncating variants was performed using a two-sided Fisher's exact test in GraphPad Prism (GraphPad Software, San Diego, CA).

Genetic analysis

The *FOXE3* coding region (NM_012186.3) was examined by direct DNA sequencing of PCR products, using overlapping primer pairs (Supplementary Material, Table S3) as described (11), or via exome sequencing (47,48). Sanger sequencing was used to confirm variants and perform segregation analysis. Variants were assessed in comparison to the general population using gnomAD v2.1.1 (49), published *FOXE3* control data (11), and Czech population frequency data curated by the National Centre for Medical Genomics comprising 3616 exomes and 88 genomes (ncmg.cz). Homozygous genotypes were confirmed by trio segregation, TaqMan assays using probe Hs03021807_cn (Thermo Fisher Scientific; Waltham, MA), copy number assessment of exome data using VarSeq CNV Caller (Golden Helix, Inc., Bozeman, MT) or microarray analysis as previously described (50) in all but one family with known consanguinity. Pathogenic effects were evaluated using SIFT, Polyphen2, Mutation Assessor, Mutation Taster, FATHMM-MKL, Combined Annotation Dependent Depletion [CADD (Phred)] and Rare Exome Variant Ensemble Learner (REVEL) scores, implemented via dbNSFP v4.1a (51) accessed through the Ensembl Variant effect predictor (52). Pathogenicity was assessed using ACMG/AMP criteria (53). All pathogenic/-likely pathogenic variants were deposited in ClinVar, accession numbers SCV001593176–SCV001593189.

Six representative *FOXE3* variants were selected for *in silico* and functional analysis as described below: recessive p.Met82Val, p.Phe186Serfs*38, p.Glu236Serfs*71 and p.Cys240* and dominant p.Leu315Alafs*117 and p.*320Serext*72, hereafter referred to as p.Met82Val, p.Phe186fs, p.Glu236fs, p.Cys240*, p.Lue315fs and p.*320ext.

Modeling FOXE3 protein structure

3D structures for wild-type (NP_036318.1) and mutant (recessive p.Met82Val, p.Phe186fs, p.Glu236fs, p.Cys240* and dominant p.Leu315fs and p.*320ext) full-length polypeptides were modeled using I-Tasser (54) and annotated using Pymol 2.4 (55). The location of the FHD was determined based on UniProt (https://www.uniprot.org) and the NLS was identified using PredictNLS https://

rostlab.org/owiki/index.php/PredictNLS and PSORT II Prediction, https://psort.hgc.jp/form2.html.

Plasmids and expression constructs

Since the *FOXE3* coding segment lacks introns, wild-type and mutant alleles were amplified by PCR from genomic DNA samples using *FOXE3* primers (Supplementary Material, Table S3) and subcloned in pcDNA3.1/myc-His A (Invitrogen, Carlsbad, CA). N-terminal FLAG epitope tags were added by inserting a phosphorylated dsDNA adaptor encoding an optimal start codon, FLAG peptide and the N-terminal portion of the *FOXE3* open reading frame (Supplementary Material, Table S3) into the *Bam*HI site of *FOXE3* constructs. $FOXE3^{myc}$ constructs were generated by PCR, using *FOXE3* genomic forward and C-terminal Myc reverse primers (Supplementary Material, Table S3). All clones were verified by Sanger sequencing.

For luciferase cotransfection assays, we added FOXD3 binding sites to TK-luc reporter plasmid, which contains a minimal herpes simplex virus (HSV) thymidine kinase (TK) promoter driving *Photinus* firefly luciferase. Complementary phosphorylated oligonucleotides (Supplementary Material, Table S3) with three FOXD3 consensus binding sites (NAWTGTTTRTTT) were annealed, ligated via *Bam*HI sticky ends and inserted in the *Bam*HI site of TK-luc, upstream from the TK promoter. The resulting construct, $(FHB)_6$-TK-luc, contains six FOXD3 binding sites: 5′-GGATCCGTA**TTGTTTGTTT**AAGCACTAGG**TATTGTTATTTT**AAGCACTAGTGA**TTGTTTGTTT**AAGCAGCTAGGATCCGT**ATTGTTTGTTT**AAGCACTAGGT**ATTGTTATTTT**AAGCACTAGTG**TTTGTTTGTTA**AAGCAGCTAGGATCC.

Cell culture and transfection

Human B3 lens epithelial (HLE-B3) cells (CRL-11421, ATCC, Manassas, VA) were cultured in Minimum Essential Media (MEM) supplemented with 20% fetal bovine serum (FBS), non-essential amino acids, 1 mM Na pyruvate and penicillin/streptomycin (Thermo Fisher). HEK293 human embryonic kidney cells (CRL-1573™, ATCC) were grown in Dulbecco's Modified Eagle Medium (DMEM) supplemented with 10% FBS. Transfections were performed at 70–90% confluence with Lipofectamine 2000 reagent (Invitrogen) and harvested 48 h later.

Wild-type and mutant expression studies

To assess FOXE3 protein levels in HLE-B3 cells transfected with different FOXE3 expression constructs, we performed western blot analysis. Cells were harvested by scraping and centrifugation and lysed in 50 mM HEPES pH 7.4, 150 mM NaCl, 1 mM EGTA, 10% Glycerol 1% Triton X-100. The lysates were clarified by centrifugation for 3 min at 12 000*g*. Total cellular protein extracts were separated by 10% SDS-PAGE and transferred to the Immobilon-P PVDF membrane (Millipore Sigma, Burlington, MA). Membrane was blocked in TBST buffer containing 3% non-fat milk, stained with Ponceau S (Sigma-Aldrich) to verify equal protein loading and probed sequentially with goat anti-FOXE3 (N17) antibody (1:1000, SCBT, Santa Cruz, CA) and HRP-conjugated donkey antigoat IgG (1:2000, SCBT). Immunoreactive proteins were detected by chemiluminescence using a UVP Bioimaging System or CL-XPosure film (Thermo Fisher). FOXE3 protein levels were quantified by ImageJ densitometry ($n = 3$ representative blots), normalized to wild-type FOXE3 and plotted using Prism 9 (GraphPad, San Diego, CA). Statistical significance was assessed using an unpaired *t*-test. Results are given as mean ± standard error of the mean (SEM).

RT-PCR was performed to confirm equivalent levels of *FOXE3* mRNA. DNase-treated total RNA (1 µg) was used as the template for cDNA synthesis (SuperScript III reverse transcriptase, Invitrogen). Replicate PCRs were performed using *FOXE3* and *GAPDH* (normalization) primers (Supplementary Material, Table S3).

FOXE3 subcellular localization

HLE-B3 cells were grown on coverslips in 60-mm culture dishes and transfected in parallel with FLAG constructs corresponding to wild-type and six mutant *FOXE3* alleles, with equal amounts of plasmid DNA per dish. After 48 h, cells were fixed with 4% paraformaldehyde in phosphate-buffered saline (PBS) for 15 min at room temperature and permeabilized with 0.25% Triton X-100 PBS for 5 min. Coverslips were blocked in 10% normal goat serum in PBS at 37°C for 30 min, incubated overnight with anti-FLAG M2 antibody (1:500, Sigma-Aldrich), washed with PBS three times, incubated for 1 h with Alexa 568-conjugated donkey anti-mouse IgG (1:1000, Thermo Fisher), washed with PBS, mounted on glass slides with PermaFluor aqueous media (Thermo Fisher) containing 1 µg/ml 4′,6-diamidine-2′-phenylindole dihydrochloride (DAPI) and imaged with a fluorescence microscope. The numbers of cells with cytoplasmic and nuclear-restricted FLAG staining were counted in 10 randomly selected fields and averaged for three independent transfections per construct, with untransfected HLE-B3 cells as a negative control. The percentage of FLAG+ cells with cytoplasmic staining was plotted for each construct using GraphPad Prism 9. Statistical significance was assessed using an unpaired *t*-test. Results are given as mean ± SEM.

Electrophoretic mobility shift assays (EMSA)

DNA binding was evaluated using a 32-bp fragment containing a single forkhead domain consensus site (FHB) or a modified site in which nucleotides $TTT_{16–18}$ were replaced by $CCC_{16–18}$ (FHBmut) as EMSA probes (Supplementary Material, Table S3). Probes were prepared by end-labeling complementary oligonucleotides with biotin using terminal deoxynucleotidyl transferase (Pierce 3′ end DNA labeling kit, Thermo Fisher) and slow annealing (1°C per min cooling from 95°C). Nuclear extracts from transfected HLE-B3 cells were prepared as described below and incubated with DNA probe for 20 min at 25°C. Binding reaction was performed as recommended by manufacturer. Briefly, equal volumes of nuclear extracts from each transfection and untransfected control were incubated in binding buffer [10 mM Tris, 50 mM KCl, 1 mM dithiothreitol (DTT), pH 7.5] containing 50 ng/µl of Poly(dI-dC) and 20 fmol of biotin-end-labeled target DNA. DNA-protein complexes were resolved by native 5% polyacrylamide gel electrophoresis in 0.5× TBE (Tris-borate-EDTA) at 4°C with 10 V/cm and were visualized by chemiluminescence (LightShift System, Thermo Fisher). Untransfected HLE-B3 extracts were used as a control for non-specific binding. Supershift experiments were performed by adding 1 µg FOXE3 antibody (SCBT) to binding reactions and incubating for an additional 30 min. Equal concentration of FOXE3 protein and its variants as well as equal protein loading were verified by western blot analysis, as described above.

Immunoprecipitation

HLE-B3 cells were transiently transfected with plasmids expressing wild-type or mutant FOXE3 (N-terminal FLAG tag) and wild-type FOXE3 (C-terminal myc epitope). Nuclear protein extracts were prepared with CelLytic NuCLEAR extraction kit (Sigma-Aldrich, St. Louis, MO). Briefly, cells were incubated in cold hypotonic lysis buffer for 20 min, vortexed in the presence of 0.6% Igepal CA-630, and centrifuged at 10 000 × *g*. Proteins were released from the nuclear pellet by extraction in 0.42 M NaCl in the presence of protease inhibitors (Sigma Aldrich).

For immunoprecipitation, nuclear extracts were diluted in 10 volumes equilibration buffer (20 mM HEPES pH 7.5, 1.5 mM $MgCl_2$, 10 mM KCl, 0.2 mM EDTA, 150 mM NaCl, 10% glycerol) and divided into three equal parts, which were incubated in parallel at 4°C overnight with mouse monoclonal anti-FLAG M2 (Sigma-Aldrich), anti-Myc R950-25 (Invitrogen) or normal mouse IgG (SCBT) in equal concentrations. Protein G PLUS-agarose beads (SCBT) were then added for 1 h at 4°C and washed 5 times in the cold buffer containing 50 mM HEPES, pH 7.5, 150 mM NaCl, 1.5 mM $MgCl_2$, 1 mM EDTA and 0.1% Igepal CA-630. Bound proteins were released from agarose beads by incubation at 94°C in SDS sample loading buffer containing 50 mM DTT. Western blot analysis was performed on immunoprecipitates and input protein extracts using goat anti-FOXE3 antibody as described above.

Luciferase reporter assays

The transcriptional activity of FOXE3 variants was assessed by cotransfecting HLE-B3 or HEK293 cells with *FOXE3* cDNA expression and the $(FHB)_6$-TK-luc reporter plasmids. Cells (10^5) were seeded in 24-well plates and harvested 2 days after transfection with 100 ng $(FHB)_6$-TK-luc reporter, 60 ng β-galactosidase calibration vector (pcDNA3.1/His/lacZ) and 100–900 ng pcDNA3.1-FOXE3 expression vector per well. We adjusted the amount of expression plasmid DNA to achieve comparable levels of wild-type or mutant FOXE3 protein in nuclear extracts (100 ng for wild-type FOXE3 and p.Met82Val, 500 ng for p.Glu236fs, p.Cys240*, p.Leu315fs, p.*320ext and 900 ng for p.Phe186fs) but kept the total amount of DNA per transfection constant (900 ng/per well) by adding empty pcDNA3.1 vector DNA. Luciferase activity was normalized to β-galactosidase, and both enzyme assays were performed using commercial reagents (Promega, Madison, WI). Fold-transactivation was calculated relative to pcDNA control transfections, in which the *FOXE3* expression vector was replaced with empty pcDNA3.1 vector. All transfection experiments were repeated at least three times, with triplicate wells per experiment. Results ±SEM were plotted using GraphPad Prism 9. Statistical significance was assessed using an unpaired *t*-test.

Supplementary Material

Supplementary Material are available at *HMGJ* online.

Acknowledgements

The authors are grateful to the families who have participated in these studies. We thank Dr Nikola Jarova for referral and initial examination of Family 15 and Dr Martin Maliska for OCT imaging of family 16. We thank the Czech National Center for Medical Genomics for providing allelic frequencies in ethnically matched populations for comparison (project CZ.02.1.01/0.0/0.0/18_046/0015515).

Conflict of Interest statement. The authors have no conflict of interest to disclose.

Funding

US National Institutes of Health grants EY025718 and EY015518 to E.V.S. and EY19497 to T.G.; Children's Research Institute funds to E.V.S.; Czech Republic Ministry of Health grants 17-30500A to P.L.; Charles University institutional funding PROGRES-Q26/LF1, SVV UK260516 and UNCE/MED/007 as well as GAUK 82318 to J.M.; and the Foerderer Fund, the Robison D. Harley, MD, Endowed Chair in Pediatric Ophthalmology and Ocular Genetics, the Adeline Lutz—Steven S.T. Ching, M.D. Distinguished Professorship in Ophthalmology and an unrestricted grant from Research to Prevent Blindness to the Department of Ophthalmology at the University of Rochester to A.V.L.

References

1. Semina, E.V., Brownell, I., Mintz-Hittner, H.A., Murray, J.C. and Jamrich, M. (2001) Mutations in the human forkhead transcription factor FOXE3 associated with anterior segment ocular dysgenesis and cataracts. *Hum. Mol. Genet.*, **10**, 231–236.
2. Blixt, A., Mahlapuu, M., Aitola, M., Pelto-Huikko, M., Enerback, S. and Carlsson, P. (2000) A forkhead gene, FoxE3, is essential for lens epithelial proliferation and closure of the lens vesicle. *Genes Dev.*, **14**, 245–254.
3. Brownell, I., Dirksen, M. and Jamrich, M. (2000) Forkhead Foxe3 maps to the dysgenetic lens locus and is critical in lens development and differentiation. *Genesis*, **27**, 81–93.
4. Golson, M.L. and Kaestner, K.H. (2016) Fox transcription factors: from development to disease. *Development*, **143**, 4558–4570.
5. Ormestad, M., Blixt, A., Churchill, A., Martinsson, T., Enerback, S. and Carlsson, P. (2002) Foxe3 haploinsufficiency in mice: a model for Peters' anomaly. *Invest. Ophthalmol. Vis. Sci.*, **43**, 1350–1357.
6. Valleix, S., Niel, F., Nedelec, B., Algros, M.P., Schwartz, C., Delbosc, B., Delpech, M. and Kantelip, B. (2006) Homozygous nonsense mutation in the FOXE3 gene as a cause of congenital primary aphakia in humans. *Am. J. Hum. Genet.*, **79**, 358–364.
7. Iseri, S.U., Osborne, R.J., Farrall, M., Wyatt, A.W., Mirza, G., Nurnberg, G., Kluck, C., Herbert, H., Martin, A., Hussain, M.S. *et al.* (2009) Seeing clearly: the dominant and recessive nature of FOXE3 in eye developmental anomalies. *Hum. Mutat.*, **30**, 1378–1386.
8. Bremond-Gignac, D., Bitoun, P., Reis, L.M., Copin, H., Murray, J.C. and Semina, E.V. (2010) Identification of dominant FOXE3 and PAX6 mutations in patients with congenital cataract and aniridia. *Mol. Vis.*, **16**, 1705–1711.
9. Doucette, L., Green, J., Fernandez, B., Johnson, G.J., Parfrey, P. and Young, T.L. (2011) A novel, non-stop mutation in FOXE3 causes an autosomal dominant form of variable anterior segment dysgenesis including Peters anomaly. *EJHG*, **19**, 293–299.
10. Gillespie, R.L., O'Sullivan, J., Ashworth, J., Bhaskar, S., Williams, S., Biswas, S., Kehdi, E., Ramsden, S.C., Clayton-Smith, J., Black, G.C. and Lloyd, I.C. (2014) Personalized diagnosis and management of congenital cataract by next-generation sequencing. *Ophthalmology*, **121**, 2124–2137.e2.

11. Reis, L.M., Tyler, R.C., Schneider, A., Bardakjian, T., Stoler, J.M., Melancon, S.B. and Semina, E.V. (2010) FOXE3 plays a significant role in autosomal recessive microphthalmia. *Am. J. Med. Genet. A*, **152A**, 582–590.
12. Ali, M., Buentello-Volante, B., McKibbin, M., Rocha-Medina, J.A., Fernandez-Fuentes, N., Koga-Nakamura, W., Ashiq, A., Khan, K., Booth, A.P., Williams, G. *et al.* (2010) Homozygous FOXE3 mutations cause non-syndromic, bilateral, total sclerocornea, aphakia, microphthalmia and optic disc coloboma. *Mol. Vis.*, **16**, 1162–1168.
13. Anjum, I., Eiberg, H., Baig, S.M., Tommerup, N. and Hansen, L. (2010) A mutation in the FOXE3 gene causes congenital primary aphakia in an autosomal recessive consanguineous Pakistani family. *Mol. Vis.*, **16**, 549–555.
14. Islam, L., Kelberman, D., Williamson, L., Lewis, N., Glindzicz, M.B., Nischal, K.K. and Sowden, J.C. (2015) Functional analysis of FOXE3 mutations causing dominant and recessive ocular anterior segment disease. *Hum. Mutat.*, **36**, 296–300.
15. Plaisancie, J., Ragge, N.K., Dollfus, H., Kaplan, J., Lehalle, D., Francannet, C., Morin, G., Colineaux, H., Calvas, P. and Chassaing, N. (2018) FOXE3 mutations: genotype-phenotype correlations. *Clin. Genet.*, **93**, 837–845.
16. Chassaing, N., Causse, A., Vigouroux, A., Delahaye, A., Alessandri, J.L., Boespflug-Tanguy, O., Boute-Benejean, O., Dollfus, H., Duban-Bedu, B., Gilbert-Dussardier, B. *et al.* (2014) Molecular findings and clinical data in a cohort of 150 patients with anophthalmia/microphthalmia. *Clin. Genet.*, **86**, 326–334.
17. Chen, J., Wang, Q., Cabrera, P.E., Zhong, Z., Sun, W., Jiao, X., Chen, Y., Govindarajan, G., Naeem, M.A., Khan, S.N. *et al.* (2017) Molecular genetic analysis of Pakistani families with autosomal recessive congenital cataracts by homozygosity screening. *Invest. Ophthalmol. Vis. Sci.*, **58**, 2207–2217.
18. Garcia-Montalvo, I.A., Pelcastre-Luna, E., Nelson-Mora, J., Buentello-Volante, B., Miranda-Duarte, A. and Zenteno, J.C. (2014) Mutational screening of FOXE3, GDF3, ATOH7, and ALDH1A3 in congenital ocular malformations. Possible contribution of the FOXE3 p.VAL201MET variant to the risk of severe eye malformations. *Ophthalmic Genet.*, **35**, 190–192.
19. Habibi, I., Youssef, M., Marzouk, E., El Shakankiri, N., Gawdat, G., El Sada, M., Schorderet, D.F. and Abou Zeid, H. (2019) Mutations in VSX2, SOX2, and FOXE3 identified in patients with micro−/anophthalmia. *Adv. Exp. Med. Biol.*, **1185**, 221–226.
20. Khan, S.Y., Vasanth, S., Kabir, F., Gottsch, J.D., Khan, A.O., Chaerkady, R., Lee, M.C., Leitch, C.C., Ma, Z., Laux, J. *et al.* (2016) FOXE3 contributes to Peters anomaly through transcriptional regulation of an autophagy-associated protein termed DNAJB1. *Nat. Commun.*, **7**, 10953.
21. Pantoja-Melendez, C., Ali, M. and Zenteno, J.C. (2013) An epidemiological investigation of a Forkhead box protein E3 founder mutation underlying the high frequency of sclerocornea, aphakia, and microphthalmia in a Mexican village. *Mol. Vis.*, **19**, 1866–1870.
22. Quiroz-Casian, N., Chacon-Camacho, O.F., Barragan-Arevalo, T., Nava-Valdez, J., Lieberman, E., Salgado-Medina, A., Navas, A., Graue-Hernandez, E.O. and Zenteno, J.C. (2018) Sclerocornea-microphthalmia-aphakia complex: description of two additional cases associated with novel FOXE3 mutations and review of the literature. *Cornea*, **37**, 1178–1181.
23. Saboo, U.S., Penke, D., Mahindrakar, A., Uddaraju, M., Sankurathri, C., Gong, X., Xing, C. and Mootha, V.V. (2017) Exome sequencing reveals novel homozygous FOXE3 mutation in microphthalmos with staphylomatous malformation. *Ophthalmic Genet.*, **38**, 295–297.
24. Taha Najim, R., Topa, A., Jugard, Y., Casslen, B., Odersjo, M. and Andersson Gronlund, M. (2020) Children and young adults with anophthalmia and microphthalmia: diagnosis and management. *Acta Ophthalmol.*, **98**, 848–858.
25. Ullah, E., Nadeem Saqib, M.A., Sajid, S., Shah, N., Zubair, M., Khan, M.A., Ahmed, I., Ali, G., Dutta, A.K., Danda, S. *et al.* (2016) Genetic analysis of consanguineous families presenting with congenital ocular defects. *Exp. Eye Res.*, **146**, 163–171.
26. Rashid, M., Qasim, M., Ishaq, R., Bukhari, S.A., Sajid, Z., Ashfaq, U.A., Haque, A. and Ahmed, Z.M. (2020) Pathogenic variants of AIPL1, MERTK, GUCY2D, and FOXE3 in Pakistani families with clinically heterogeneous eye diseases. *PLoS One*, **15**, e0239748.
27. Thanikachalam, S., Hodapp, E., Chang, T.C., Swols, D.M., Cengiz, F.B., Guo, S., Zafeer, M.F., Seyhan, S., Bademci, G., Scott, W.K. *et al.* (2020) Spectrum of genetic variants associated with anterior segment dysgenesis in South Florida. *Genes (Basel)*, **11**, 350.
28. Patel, A., Hayward, J.D., Tailor, V., Nyanhete, R., Ahlfors, H., Gabriel, C., Jannini, T.B., Abbou-Rayyah, Y., Henderson, R., Nischal, K.K. *et al.* (2019) The Oculome panel test: next-generation sequencing to diagnose a diverse range of genetic developmental eye disorders. *Ophthalmology*, **126**, 888–907.
29. Zhang, X.H., Da Wang, J., Jia, H.Y., Zhang, J.S., Li, Y., Xiong, Y., Li, J., Li, X.X., Huang, Y., Zhu, G.Y. *et al.* (2018) Mutation profiles of congenital cataract genes in 21 northern Chinese families. *Mol. Vis.*, **24**, 471–477.
30. Jin, C., Marsden, I., Chen, X. and Liao, X. (1999) Dynamic DNA contacts observed in the NMR structure of winged helix protein-DNA complex. *J. Mol. Biol.*, **289**, 683–690.
31. Chen, X., Wei, H., Li, J., Liang, X., Dai, S., Jiang, L., Guo, M., Qu, L., Chen, Z., Chen, L. *et al.* (2019) Structural basis for DNA recognition by FOXC2. *Nucleic Acids Res.*, **47**, 3752–3764.
32. Li, J., Dantas Machado, A.C., Guo, M., Sagendorf, J.M., Zhou, Z., Jiang, L., Chen, X., Wu, D., Qu, L., Chen, Z. *et al.* (2017) Structure of the Forkhead domain of FOXA2 bound to a complete DNA consensus site. *Biochemistry*, **56**, 3745–3753.
33. Saleem, R.A., Banerjee-Basu, S., Murphy, T.C., Baxevanis, A. and Walter, M.A. (2004) Essential structural and functional determinants within the forkhead domain of FOXC1. *Nucleic Acids Res.*, **32**, 4182–4193.
34. Stroud, J.C., Wu, Y., Bates, D.L., Han, A., Nowick, K., Paabo, S., Tong, H. and Chen, L. (2006) Structure of the forkhead domain of FOXP2 bound to DNA. *Structure*, **14**, 159–166.
35. Van Hellemont, R., Monsieurs, P., Thijs, G., de Moor, B., Van de Peer, Y. and Marchal, K. (2005) A novel approach to identifying regulatory motifs in distantly related genomes. *Genome Biol.*, **6**, R113.
36. Lamba, P., Fortin, J., Tran, S., Wang, Y. and Bernard, D.J. (2009) A novel role for the forkhead transcription factor FOXL2 in activin A-regulated follicle-stimulating hormone beta subunit transcription. *Mol. Endocrinol.*, **23**, 1001–1013.
37. Singh, P., Han, E.H., Endrizzi, J.A., O'Brien, R.M. and Chi, Y.I. (2017) Crystal structures reveal a new and novel FoxO1 binding site within the human glucose-6-phosphatase catalytic subunit 1 gene promoter. *J. Struct. Biol.*, **198**, 54–64.
38. Schimmel, J., Eifler, K., Sigurethsson, J.O., Cuijpers, S.A., Hendriks, I.A., Verlaan-de Vries, M., Kelstrup, C.D., Francavilla, C.,

Medema, R.H., Olsen, J.V. *et al.* (2014) Uncovering SUMOylation dynamics during cell-cycle progression reveals FoxM1 as a key mitotic SUMO target protein. *Mol. Cell*, **53**, 1053–1066.
39. Perumal, K., Dirr, H.W. and Fanucchi, S. (2015) A single amino acid in the hinge loop region of the FOXP Forkhead domain is significant for dimerisation. *Protein J.*, **34**, 111–121.
40. Chaurasia, S., Jakati, S., Ramappa, M., Mishra, D.K. and Edward, D.P. (2020) Anterior segment alterations in congenital primary aphakia-a clinicopathologic report of five cases. *Indian J. Ophthalmol.*, **68**, 1564–1568.
41. Blixt, A., Landgren, H., Johansson, B.R. and Carlsson, P. (2007) Foxe3 is required for morphogenesis and differentiation of the anterior segment of the eye and is sensitive to Pax6 gene dosage. *Dev. Biol.*, **302**, 218–229.
42. Kahrizi, K., Hu, H., Hosseini, M., Kalscheuer, V.M., Fattahi, Z., Beheshtian, M., Suckow, V., Mohseni, M., Lipkowitz, B., Mehvari, S. *et al.* (2019) Effect of inbreeding on intellectual disability revisited by trio sequencing. *Clin. Genet.*, **95**, 151–159.
43. Kuang, S.Q., Medina-Martinez, O., Guo, D.C., Gong, L., Regalado, E.S., Reynolds, C.L., Boileau, C., Jondeau, G., Prakash, S.K., Kwartler, C.S. *et al.* (2016) FOXE3 mutations predispose to thoracic aortic aneurysms and dissections. *J. Clin. Invest.*, **126**, 948–961.
44. Saleem, R.A., Banerjee-Basu, S., Berry, F.B., Baxevanis, A.D. and Walter, M.A. (2003) Structural and functional analyses of disease-causing missense mutations in the forkhead domain of FOXC1. *Hum. Mol. Genet.*, **12**, 2993–3005.
45. Morris, G., Stoychev, S., Naicker, P., Dirr, H.W. and Fanucchi, S. (2018) The forkhead domain hinge-loop plays a pivotal role in DNA binding and transcriptional activity of FOXP2. *Biol. Chem.*, **399**, 881–893.
46. Stenson, P.D., Mort, M., Ball, E.V., Chapman, M., Evans, K., Azevedo, L., Hayden, M., Heywood, S., Millar, D.S., Phillips, A.D. *et al.* (2020) The human gene mutation database (HGMD((R))): optimizing its use in a clinical diagnostic or research setting. *Hum. Genet.*, **139**, 1197–1207.
47. Reis, L.M., Sorokina, E.A., Thompson, S., Muheisen, S., Velinov, M., Zamora, C., Aylsworth, A.S. and Semina, E.V. (2019) De novo missense variants in WDR37 cause a severe multisystemic syndrome. *Am. J. Hum. Genet.*, **105**, 425–433.
48. Dudakova, L., Skalicka, P., Ulmanova, O., Hlozanek, M., Stranecky, V., Malinka, F., Vincent, A.L. and Liskova, P. (2020) Pseudodominant nanophthalmos in a Roma family caused by a novel PRSS56 variant. *J. Ophthalmol.*, **2020**, 6807809.
49. Karczewski, K.J., Francioli, L.C., Tiao, G., Cummings, B.B., Alfoldi, J., Wang, Q., Collins, R.L., Laricchia, K.M., Ganna, A., Birnbaum, D.P. *et al.* (2020) The mutational constraint spectrum quantified from variation in 141,456 humans. *Nature*, **581**, 434–443.
50. Schilter, K.F., Reis, L.M., Schneider, A., Bardakjian, T.M., Abdul-Rahman, O., Kozel, B.A., Zimmerman, H.H., Broeckel, U. and Semina, E.V. (2013) Whole-genome copy number variation analysis in anophthalmia and microphthalmia. *Clin. Genet.*, **84**, 473–481.
51. Liu, X., Jian, X. and Boerwinkle, E. (2013) dbNSFP v2.0: a database of human non-synonymous SNVs and their functional predictions and annotations. *Hum. Mutat.*, **34**, E2393–E2402.
52. McLaren, W., Gil, L., Hunt, S.E., Riat, H.S., Ritchie, G.R., Thormann, A., Flicek, P. and Cunningham, F. (2016) The Ensembl variant effect predictor. *Genome Biol.*, **17**, 122.
53. Richards, S., Aziz, N., Bale, S., Bick, D., Das, S., Gastier-Foster, J., Grody, W.W., Hegde, M., Lyon, E., Spector, E. *et al.* (2015) Standards and guidelines for the interpretation of sequence variants: a joint consensus recommendation of the American College of Medical Genetics and Genomics and the Association for Molecular Pathology. *Genetics in medicine: official journal of the American College of Medical Genetics*, **17**, 405–424.
54. Yang, J., Yan, R., Roy, A., Xu, D., Poisson, J. and Zhang, Y. (2015) The I-TASSER suite: protein structure and function prediction. *Nat. Methods*, **12**, 7–8.
55. *The PyMOL Molecular Graphics System, Version 2.0*. Schrödinger, LLC.